AIAA Aviation Forum and ASCEND co-located Conference Proceedings
29 July - 2 August 2024, Las Vegas, Nevada
AIAA AVIATION FORUM AND ASCEND 2024

10.2514/6.2024-3587

Trajectory Optimization of eVTOL and Conventional Aircraft: A Comparative Analysis of Vortex Particle Method and Vortex Lattice + Blade Element Momentum Theory

Andrew Tagg *, Ryan Anderson†, Cibin Joseph‡, Andrew Ning§
Brigham Young University, Provo, UT 84602

Trajectory optimization of aircraft transition maneuvers can significantly influence the design of these systems, particularly when making decisions about aircraft geometry, propulsion sizing, and control system design. This paper presents the trajectory optimization of air vehicles including electric vertical takeoff and landing (eVTOL) as well as conventional aircraft. The study evaluates the influence of fidelity in trajectory design by comparing the use of two aerodynamic methods in the context of trajectory optimization. The mid-fidelity method utilizes a vortex lattice method (VLM) to model lifting surfaces while employing blade element momentum theory (BEMT) to model rudimentary rotor-wing interactions. The high-fidelity approach applies a vortex particle method (VPM) to model the wing and propeller geometries while capturing more complex wake interactions. This work also presents a trajectory optimization methodology that is well suited for high fidelity VPM simulations and overcomes many of the challenges associated with traditional methods such as robust convergence and computational cost. The new method is validated through a case study which leverages the VLM-BEMT model to compare results with that of a traditional shooting method. The method is then employed to optimize trajectories using the VPM to model both conventional and eVTOL aircraft.

I. Introduction

Electric vertical lift technology has emerged as a promising field in the aeronautical industry with potential to deliver advanced capabilities and impact many aspects of society. The transition between hover and cruise, however, presents a challenging engineering problem. This is partly because the largest power requirement of the aircraft occurs during the hover and transition stage, and drives the engine and battery sizing. Additionally, modeling the aerodynamics of this phase of the flight trajectory is significantly difficult due to wake interactions and potential for wake instability. The objective of the present study is to optimize the control and resulting trajectory of the eVTOL transition.

One of the main challenges of eVTOL trajectory optimization is the cost of accurately modeling the aerodynamics, particularly of the propulsion system. These often involve distributed electric propulsion with tilt-wing or tilt-rotor mechanisms, resulting in significant wake interactions between rotors and wings. Aerodynamic models used in trajectory optimization typically utilize empirical expressions or stability derivative based simplifications in order to keep simulation times small and to make use of robust collocation methods [1–3]. These models have also been used in takeoff-to-cruise trajectory optimization of tandem tilt-wing eVTOL aircraft [4]. The dynamics of the propulsion system have also been incorporated into similar problems by utilizing a simplified battery cell model [5]. Unfortunately, such simplified aerodynamic models either heavily rely on the accuracy of empirical expressions or do not fully capture these complex wake interactions, making them unsuitable for optimizing the eVTOL transition maneuver. Hover and climb phases also typically require the most power input in the mission profile, while power demand during the cruise phase is relatively low and stable, making accurate modeling of the transition maneuver crucial [6, 7]. The forces and torques during these phases dictate engine sizing and battery capacity. If higher-fidelity models are used, the time resolution required for modeling the rotors results in long simulation times. Often a trade-off has to be made when modeling these configurations.

Another challenge of eVTOL trajectory optimization is the choice of objective function and constraints that impact the desired performance and feasibility of the trajectories. For example, Wang et al. generated minimum-time trajectories

*Doctoral Student, Mechanical Engineering, AIAA Student Member
†Doctoral Candidate, Mechanical Engineering, AIAA Student Member
‡Post Doctoral Scholar, Mechanical Engineering, AIAA Student Member
§Associate Professor, Mechanical Engineering, AIAA Associate Fellow

for an eVTOL aircraft using straight lines and circular arcs called 'motion-primitives' [8]. Chauhan and Martins considered stall and acceleration constraints in their optimization problem and found that the optimal takeoffs involve stalling the wings or flying close to the stall angle of attack [4]. Investigation into wind-optimal trajectories have also been conducted on an eVTOL multirotor aircraft to study the influence on energy consumption and operational benefits [9]. These works show that various objectives, constraints, and methodologies for trajectory optimization can lead to equally valid, though significantly different optimal trajectories.

Different trajectory optimization approaches also come with their own set of challenges. One example is shooting methods, which consist of suggesting a set of control inputs as a function of time, simulating the trajectory, evaluating a cost function, and then iterating. They are easy to implement, but often suffer from poor convergence, leading to an excessive number of function calls or even failure to converge. Collocation methods are another approach in which all state variables throughout the trajectory are prescribed, and constraints are implemented which enforce the system's governing equations. These methods tend to be computationally less expensive and more numerically stable. Researchers have presented comparisons between different collocation methods, like those by Wang et al. to quantify the advantages of a dynamic model that is reformulated in terms of propulsive capacity. Anderson et al. also utilizes collocation to optimize the trajectory of a bi-wing tail sitter configuration and compare the results of low-fidelity and mid-fidelity models [10]. The result was significantly different trajectory paths between the various methods. Li et al., used quasi-steady lift polars in a collocation approach to optimize the transition trajectory of a tail-sitter VTOL aircraft [11]. While collocation seems like an attractive option, it typically requires quasi-steady models that do not depend on time history. Unfortunately, use of quasi-steady models inherently ignores unsteady wake interactions. In order to capture these interactions, one must include not only vehicle states, but wake states in the design variables of the collocation. This makes collocation more intractable for methods like the VPM, which requires at least 18 states per particle per time step. This often amounts to millions of states that need to be prescribed in the collocation, making this approach immensely computationally expensive.

Efforts have been made to incorporate unsteady wake effects into trajectory optimization using the VPM. Droandi et al. used VPM to build a surrogate model, from which he optimized a series of trim points for the transition of Airbus eVTOL Vahana [12]. While useful, this neglects the effect of wake interactions across time steps. Robertson and Reich optimized perching maneuvers of a flat plate with a fully unsteady vortex particle wake model using a shooting method and a genetic algorithm, noting they had reached the limit of what was computationally practical for optimization [13].

The present work adopts a nested trajectory optimization method that allows for the incorporation of fully unsteady, computationally expensive models like VPM without sacrificing robustness. An inner-outer loop approach is implemented. The outer loop is a path planning optimization in which a reference trajectory is prescribed at each iteration. The inner loop is an optimal control problem which solves for control inputs that achieve the reference path prescribed in the outer loop. The advantage of this approach is that the outer loop is reduced to just one or two states, delegating the highly nonlinear control input problem to the inner loop. This approach will be shown to improve robustness and reduce computational cost of trajectory optimization, making it possible to employ expensive, high fidelity models to capture unsteady wake interactions that are prevalent in complex transition maneuvers. This will allow complex aerodynamics to inform the creation of more feasible and optimal trajectories, which will in turn drive the design of better aircraft systems.

II. Aircraft Models

This work features two aircraft configurations that were utilized for trajectory optimization. The first is a conventional aircraft similar to the Cessna-210 Centurion. This is a classic configuration that is mainly used as a test case in preparation for more complex geometries. The second aircraft is inspired by the Aurora Personal Air Vehicle by Boeing which is an eVTOL lift+cruise design. Geometric specifications of these aircraft are provided in the following sections.

A. Cessna-210 Geometry

The Cessna-210 aircraft model has a single 3-bladed propeller, a main wing and horizontal stabilizer as shown in Fig. 1. The fuselage and vertical tail were not modeled in the aerodynamic solvers as the aircraft was constrained to a longitudinal plane. The elevator was assumed to be 30% of the tail chord length. Since the propeller geometry was not available, a generic 3-bladed propeller model with NACA 4412 sections was used. The basic aircraft dimensions are outlined in Table 1. Control inputs provided to the aircraft were the propeller angular velocity Ω and elevator deflection

δ as given in Eq. (1).

$$\boldsymbol{u} = \begin{bmatrix} \Omega \\ \delta \end{bmatrix} \tag{1}$$

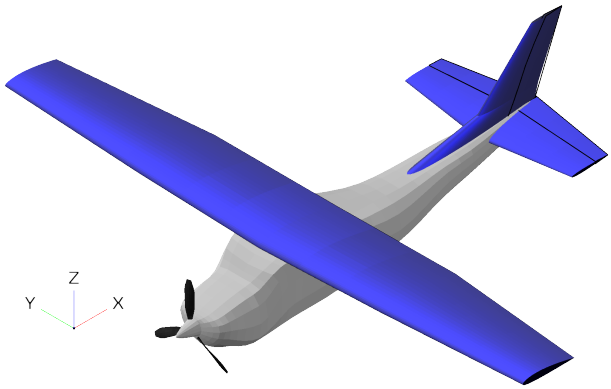

Fig. 1 OpenVSP model of the Cessna geometry

Parameter	Value
Wing span (m)	11.2
Wing root chord (m)	1.68
Wing tip chord (m)	1.22
Wing incidence (deg)	2.50
Tail span (m)	3.96
Tail root chord (m)	0.98
Tail tip chord (m)	0.68
Tail sweep angle (deg)	8.62
Rotor diameter (m)	2.04
Rotor airfoil	NACA 4412

Table 1 Cessna model dimensions

B. Lift+Cruise eVTOL Geometry

The eVTOL aircraft geometry was inspired by the Aurora PAV. It features eight 2-bladed lifter rotors and one 5-bladed pusher rotor. Airfoil profile and exact dimensions were unavailable for this model and estimates were used from images or representations. A figure of this eVTOL model is shown in Fig. 2 and dimensions can be found in Table 2. Since the analysis performed here is constrained to the longitudinal plane, the four lifter rotors in front of the wing were assumed to run at the same angular velocity. The same applies to the four lift rotors behind the wing. In addition to the two sets of lift rotors, a pusher rotor is also present on the model. The control vector for the model hence contains three angular velocities as shown in Eq. (2).

$$\boldsymbol{u} = \begin{bmatrix} \Omega_{\text{front}} \\ \Omega_{\text{rear}} \\ \Omega_{\text{pusher}} \end{bmatrix} \tag{2}$$

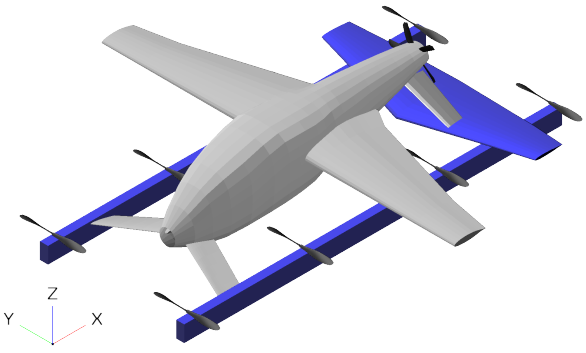

Fig. 2 OpenVSP model of the eVTOL geometry

Parameter	Value
Wing span (m)	8.53
Wing root chord (m)	1.94
Wing tip chord (m)	0.76
Wing incidence (deg)	0.00
Tail span (m)	5.16
Tail root chord (m)	1.57
Tail tip chord (m)	0.67
Lift rotor diameter (m)	1.58
Pusher rotor diameter (m)	1.21
Rotor airfoil	NACA 4412

Table 2 eVTOL model dimensions

III. Mathematical Models

A. Aerodynamic Modeling

Aircraft simulation is dependent upon the ability to evaluate forces that act on the system. It is also necessary to model the amount of power the system is using at any given time. The following aerodynamic methods are employed in order to model forces and power.

1. Vortex Lattice Method (VLM)

An unsteady vortex lattice method is used for mid-fidelity aerodynamic modeling. Both lifting surfaces and the wake are modeled using quadrilateral vortex ring elements comprising of rectilinear vortex filaments. Aerodynamic outputs including forces and moments are computed using the Kutta-Joukowski theorem shown in Eq. (3).

$$F' = \rho V \times \Gamma \tag{3}$$

where ρ is fluid density, Γ is vortex strength, V is total velocity given by

$$V = V_\infty - \Omega \times r_b + V_{\text{ind}} + V_{\text{other}} \tag{4}$$

Eq. (4) represents velocity due to the freestream, rigid body motion, wing induced vortices, and any other source. The wing geometry is discretized into vortex ring elements, each with a horseshoe vortex attached to it and the flow tangency boundary condition is imposed at a collocation point on each of the panels. The resulting system of linear equations is solved to obtain the panel circulation strengths Γ and the Biot-Savart law is utilized to find induced velocities V_{ind}. The wake generated from the trailing edge of the lifting surface is convected away at the local velocity at each time step. The Julia package VortexLattice.jl* is used in this work and more detailed descriptions of this method can be found in several aerodynamics resources [14]. Steady-state results from this method were validated using AVL† and unsteady results were compared against results from standard textbooks [14].

2. Blade Element Momentum Theory (BEMT)

Blade element momentum theory predicts the induced velocity distribution at the rotor disk under steady-state conditions. It does this by considering annular sections of the rotor disk and equating the sectional force and torque predicted by the blade element and momentum theory principles. Expressions for thrust and torque at radial sections can be obtained in terms of the induced velocity and radial location. To account for sectional blade geometry, we use tabulated airfoil lift and drag coefficients. While simple in theory, BEMT implementations are vulnerable to numerical error and exhibit lack of convergence at certain flight conditions. In this work, we use the BEMT package CCBlade‡ that has guaranteed convergence and specialized design tailored for optimization solvers.

We couple BEMT with VLM in the same way as Moore and Ning [15] by applying the velocities solved in BEMT to the control points of VLM directly behind each rotor. We include the same correction factor to account for wake development.

3. Vortex Particle Method (VPM)

The vortex particle method (VPM) is capable of modeling complex wake dynamics at orders-of-magnitude reduction in computational cost when compared with traditional mesh-based CFD approaches. The fluid vorticity is discretized through the use of vortex particles, which are governed by Eq. (5):

$$\frac{D\omega}{Dt} = (\omega \cdot \nabla)v + \nu\nabla^2 v \tag{5}$$

This approach does not require the fluid domain to be meshed; rather, vortex particles are placed only in regions of significant vorticity, thereby reducing cost. This also avoids the numerical dissipation in regions of high vorticity that is common in mesh-based approaches. In this work, we use FLOWUnsteady [16] for the high-fidelity simulations which utilizes a reformulation of the classical vortex particle method that preserves angular momentum and offers better

*github.com/byuflowlab/VortexLattice.jl
†web.mit.edu/drela/Public/web/avl
‡github.com/byuflowlab/CCBlade.jl

numerical stability characteristics compared to traditional implementations. The aircraft geometry is modeled using an actuator line approach to calculate lift and drag.

FLOWUnsteady utilizes a fast multi pole method to reduce the time complexity of the simulations from $O(n^2)$ to $O(n)$ with n vortex particles in the domain. Additionally, as vortex particles far downstream do not affect the force distribution on the aircraft, a far-field wake treatment, where the wake is cut off after 2 span lengths, was applied to reduce computational time. To avoid transients influencing the solution, simulations were started from steady-state flow solutions.

4. Power Modeling

For this project, trajectories are optimized for minimum energy consumption. As such, a method for modeling the power input to the system is needed. A basic power model is used in this work. In both the VLM-BEMT and the VPM, power is expressed as shown in Eq. (6) where Ω is rotor velocity in radians per second, and Q is the rotor torque, which is an output from the BEMT as well as the VPM aerodynamic solvers.

$$P = Q\Omega \tag{6}$$

As shown in Eq. (7), energy consumption is the time integral of power.

$$E = \int_{t_0}^{t_{\text{end}}} P dt \tag{7}$$

B. Optimization

As noted, the main goal of this project is to optimize the trajectories and corresponding control inputs of the two aforementioned aircraft. A nested optimization approach is applied to solve this problem. In the outer loop, a reference flight path is defined. In the inner loop, an optimal control method is used to fly that reference path. Using this scheme, the optimal flight path is determined based on an objective of minimum energy consumed. The outer and inner loop methodologies are described in more detail in the following sections.

1. Outer Loop Path Optimization

The path optimization is responsible for finding an optimal set of states that results in the minimum energy consumed given a set of constraints. This problem is written formally in Eq. (8)

$$\begin{aligned} \text{minimize} \quad & E \\ \text{by varying} \quad & x_{\text{ref}} \\ \text{subject to} \quad & x, u, E = \text{InnerLoop}(x_{\text{ref}}) \\ & u_{\min} \leq u \leq u_{\max} \end{aligned} \tag{8}$$

where E is the total energy consumption of the simulation, and x_{ref} is the prescribed state trajectory determined by the outer loop.

Assuming the InnerLoop() is implemented, it can be used to calculate the optimal control inputs u, the resulting actual flown path x, and the total energy E. In addition, the control inputs calculated by the inner loop must lie within the system's physical limits to prevent the outer loop from commanding infeasible paths. In the case of the Aurora PAV, all lifting rotors where confined to below 400 radians per second and the pusher rotor was confined to below 550 radians per second. In the case of the Cessna-210, the rotor was required to be below 350 radians per second, and the elevator was restricted to between -20 and 20 degrees.

Gradients are obtained using forward-mode algorithmic differentiation (AD). As our code is written entirely in the Julia language[§], the ForwardDiff [17] package provides derivatives with very little developmental effort. It is well-known that forward mode AD scales poorly with large numbers of design variables; however, in the present formulation, very few design variables are required to describe the outer-loop reference flight path. Forward-mode allows us to add an arbitrary number of constraints without additional cost for obtaining gradients. It also avoids the large memory cost of reverse-mode, which is significant when using the VPM.

[§]https://julialang.org

2. Inner Loop Optimal Control

The inner loop is responsible for calculating control inputs necessary to follow the prescribed reference path while minimizing control effort. This optimal controller is a discrete, finite horizon, linear quadratic regulator (LQR). The formulation of a basic LQR controller is shown below in Eq. (9)

$$\begin{aligned} \text{minimize} \quad & u^T R u \\ \text{by varying} \quad & u \\ \text{subject to} \quad & x_{k+1} = A x_k + B u_k \\ & x_{\text{end}} = x_{\text{ref}}(t_{\text{end}}) \end{aligned} \tag{9}$$

Where R is a matrix that defines a quadratic penalty on control effort, A and B are the result of the linearized system equations of motion, and x_{ref} is the desired path which will be provided by the outer loop. Here the subscript *end* represents the final time step of the finite horizon, not the final time step of the whole simulation. Path following is ensured by constraining the final state in the horizon, x_{end} to be the desired state corresponding to that moment in time, $x_{ref}(t_{end})$. Note also that x and u are vector functions of time. Therefore the objective function projected over the entire horizon becomes

$$O = [u_0^T u_1^T ...] \begin{bmatrix} R & & \\ & \ddots & \\ & & R \end{bmatrix} \begin{bmatrix} u_0 \\ u_1 \\ \vdots \end{bmatrix}$$

Likewise, the linearized equations of motion over the time horizon become

$$\begin{bmatrix} x_1 \\ x_2 \\ \vdots \end{bmatrix} = \begin{bmatrix} 0 & & & \\ A & \ddots & & \\ & \ddots & 0 & \\ & & A & 0 \end{bmatrix} \begin{bmatrix} x_1 \\ x_2 \\ \vdots \end{bmatrix} + \begin{bmatrix} B & & \\ & \ddots & \\ & & B \end{bmatrix} \begin{bmatrix} u_0 \\ u_1 \\ \vdots \end{bmatrix} + \begin{bmatrix} A \\ 0 \\ \vdots \end{bmatrix} x_0$$

Since this is a quadratic objective with linear constraints, it is classified as a quadratic programming (QP) problem. This problem is solved at every time step to ensure good closed loop control. Using this formulation, the process of the inner control loop is outlined below

1) Obtain desired path $x_{\text{ref}}(t)$ from outer optimization loop
2) Solve the QP problem described above
3) Extract the first control input u_0 and discard the rest
4) Propagate the system 1 time step using full nonlinear dynamics
5) Repeat steps 2-4 at every time step

Note that the QP formulation has an analytic solution, and the LQR amounts to solving one linear system of equations at every time step. Because of this, the need to calculate gradients for the inner loop is avoided completely.

IV. Results

A. Model Comparison

In order to highlight the capabilities of the VPM in capturing unsteady wake interactions, a simulation was run modeling the eVTOL configuration during a takeoff transition maneuver. First, the inner loop controller was used to fly the aircraft through the trajectory using VLM-BEMT to calculate aerodynamic forces. Then the same exact trajectory was run through a VPM simulation. This time no active control was done, but rather the state and control inputs where prescribed to be the same exact ones from the VLM-BEMT simulation. This allowed for a comparison between aerodynamic forces computed by both methods. These results include values for total lift, total drag, and thrust values for front, back, and pusher rotors. The comparisons are shown in Figs. 3 to 5.

The VLM-BEMT when compared with the VPM shows consistent trends, and reasonable average values for these aerodynamics forces. However, it lacks the ability to calculate relevant changes in lift, drag, and thrust from time step to time step. This is because there are no unsteady loads calculated in the VLM-BEMT, which leads to smoother

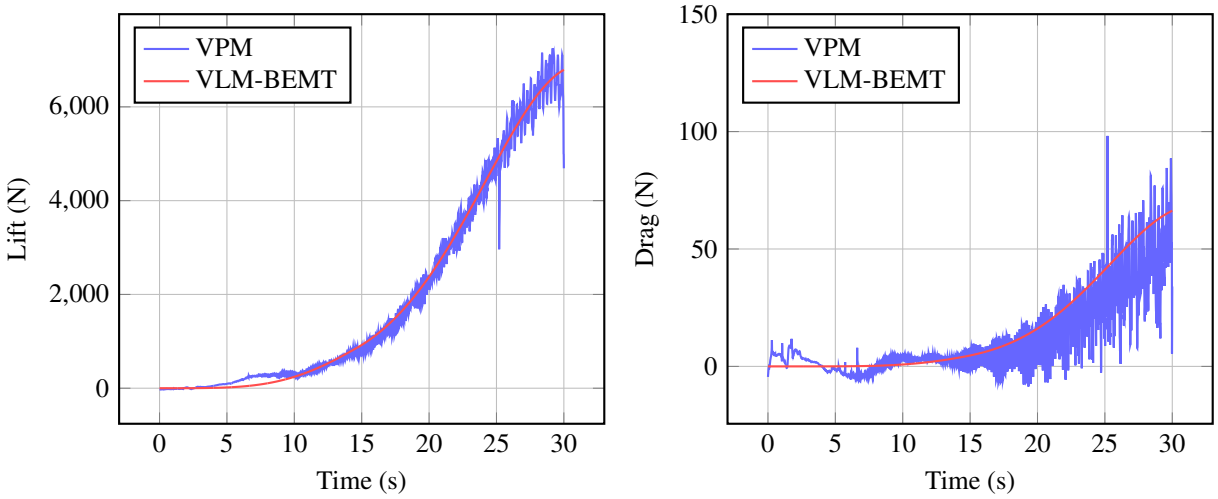

(a) Net lift (N) **(b) Net drag (N)**

Fig. 3 Comparison between VPM and VLM-BEMT lift and drag

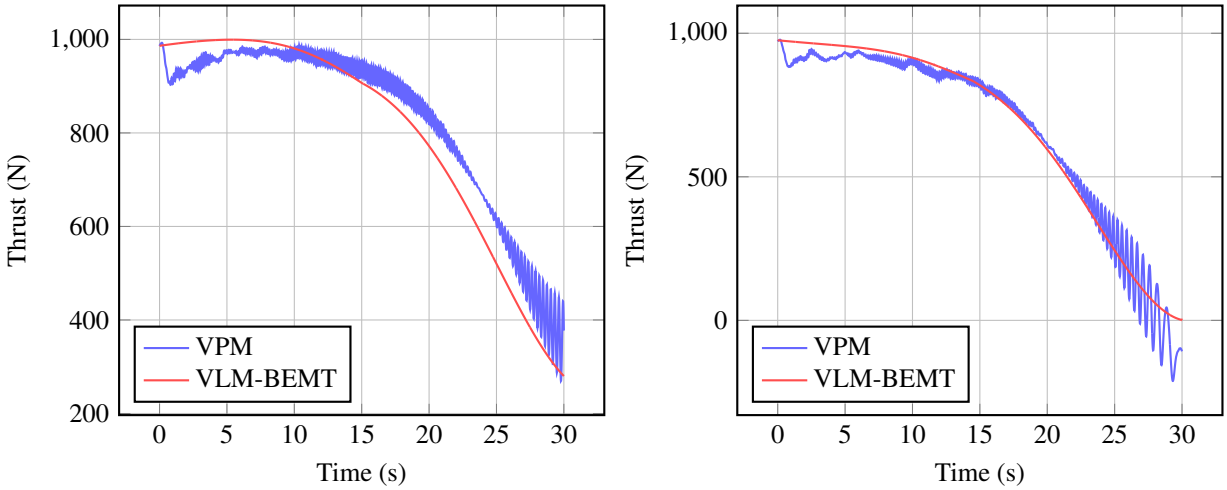

(a) Front lifter rotor thrust (N) **(b) Rear lifter rotor thrust (N)**

Fig. 4 Comparison between VPM and VLM-BEMT lifter rotor thrusts

results, but does not fully capture all of the physics involved in a complex maneuver such as the eVTOL takeoff. The VPM on the other hand shows roughly the same overall trends, and also resolves unsteady, oscillatory forces due to it's vortex particle wake modeling. Note that the oscillations are very prominent for the lifting rotors, which experience wake mixing and edgewise flow as the aircraft transitions to cruise. These unsteady forces can potentially cause large moments as well, which will further enhance the discrepancy between the two models. These results seem to suggest that for eVTOL transition maneuvers in which a high degree of wake interaction is likely to occur, the VPM will capture physical phenomenon that the VLM-BEMT will not.

B. Optimization Method Comparison

The nested trajectory optimization scheme described above was tested and compared against a traditional shooting method to evaluate its effectiveness. In both methods, Akima splines where used to discretize the design variables. This gives the advantage of being able to use relatively few design variables to describe complex curves. In the case of the nested optimization, it was possible to use as few as one spline point since the beginning and end state are fixed. As the

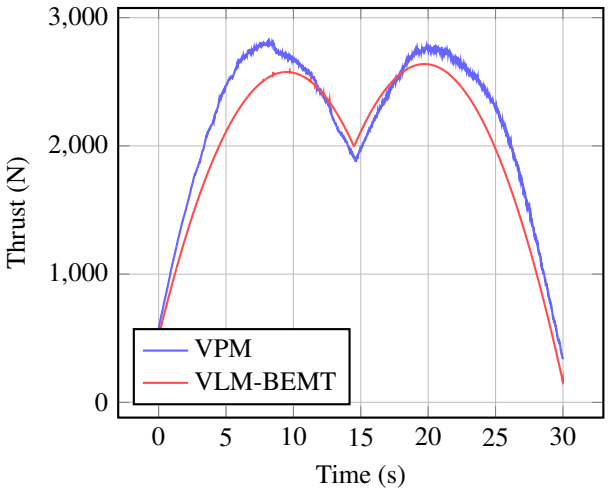

Fig. 5 Comparison of VPM, and BEMT pusher thrust

outer loop explores the design space, the spline point varies as shown in Fig. 6. Note that in this example the derivatives at the beginning and end points are constrained to zero because the aircraft is travelling from trimmed hover to trimmed cruise.

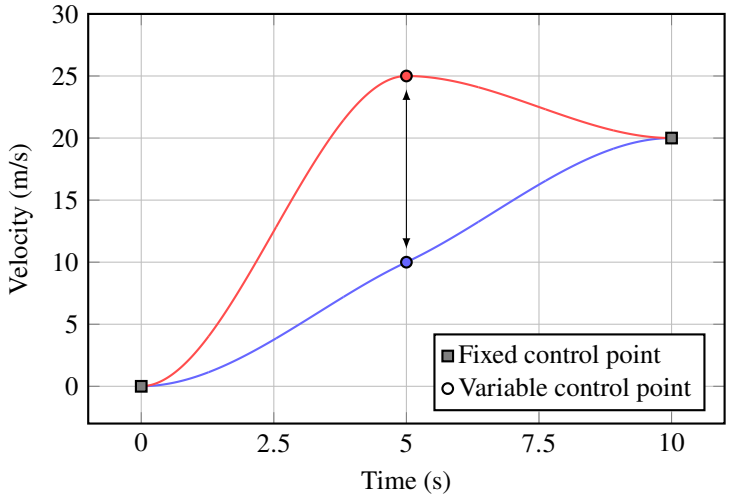

Fig. 6 Example of the Akima spline implementation with a fixed spline control point at the beginning and end of the trajectory. The variable spline control point is shown at 5 s at velocities 10 m/s and 25 m/s.

In order to compare these two methods, the VLM-BEMT was used to optimize trajectories for the eVTOL aircraft. Figure 7 compares the number of function calls in these optimizations with varying number of spline points between the two methods, and Fig. 8 compares objective function values that were achieved. For a no. of spline points less than 4, the shooting method failed to converge. The optimal control method, however, exhibited robust convergence and convergence to lower objective function magnitudes.

As shown the optimal control method consistently outperforms the shooting method both in number of function calls and final objective function value. A visual representation of a constraint function for the two methods shows a much smoother and more robust design space when compared to the shooting method. In Fig. 9, g_4 is the stall constraint, and x_1 and x_2 are two of the design variables. Note that for this example, the stall constraint was implemented to demonstrate the difference between these two methods, but for the general formulation this constraint was not used. This visualization highlights the advantage of the nested optimal control scheme over the shooting method which is highly

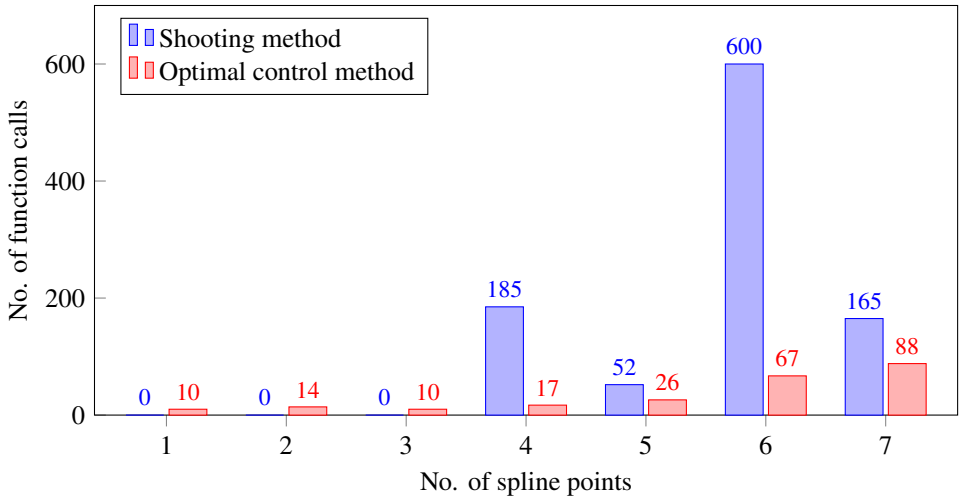

Fig. 7 Number of function calls (lower better) that was required for the shooting and optimal control methods. For a no. of spline points less than 4, the shooting method failed to converge.

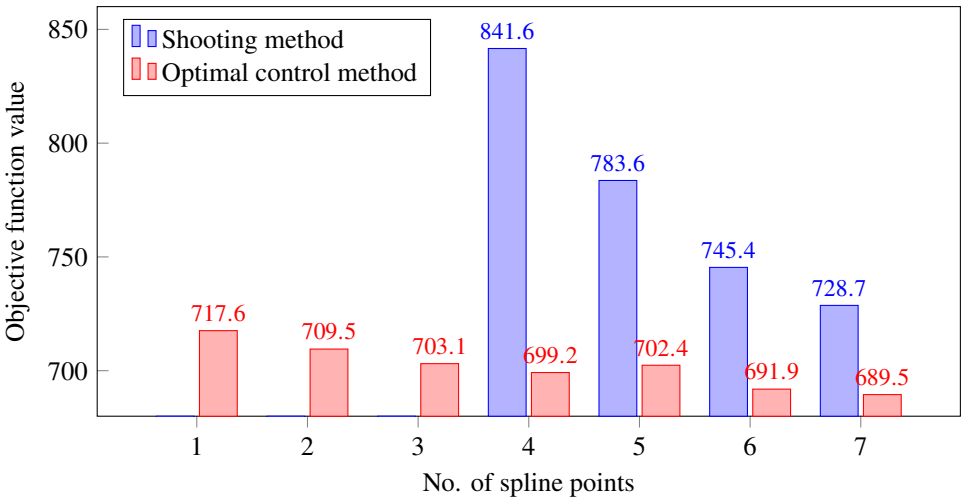

Fig. 8 Magnitude of objective function (lower better) that was achieved for the shooting and optimal control methods. For a no. of spline points less than 4, the shooting method failed to converge.

vulnerable to infeasibility. By significantly smoothing out the design space, the nested method reduces the amount of local minima, and leads to reliable and fast convergence. Because it tends to converge quickly, this method is ideal for use with high cost models such as the VPM.

C. VPM Trajectory Optimization

Because the nested trajectory optimization strategy outlined above is significantly cheaper in terms of function evaluations than other methods, it is an ideal candidate for trajectory optimization with expensive, high fidelity models like the VPM. Transition maneuvers for both the Cessna-210, and the eVTOL aircraft were optimized using the methods described above. These results highlight the effectiveness of the VPM as a tool for modeling unsteady aerodynamics. They also showcase the described methods for trajectory optimization, which demonstrate robust convergence and control for these aircraft.

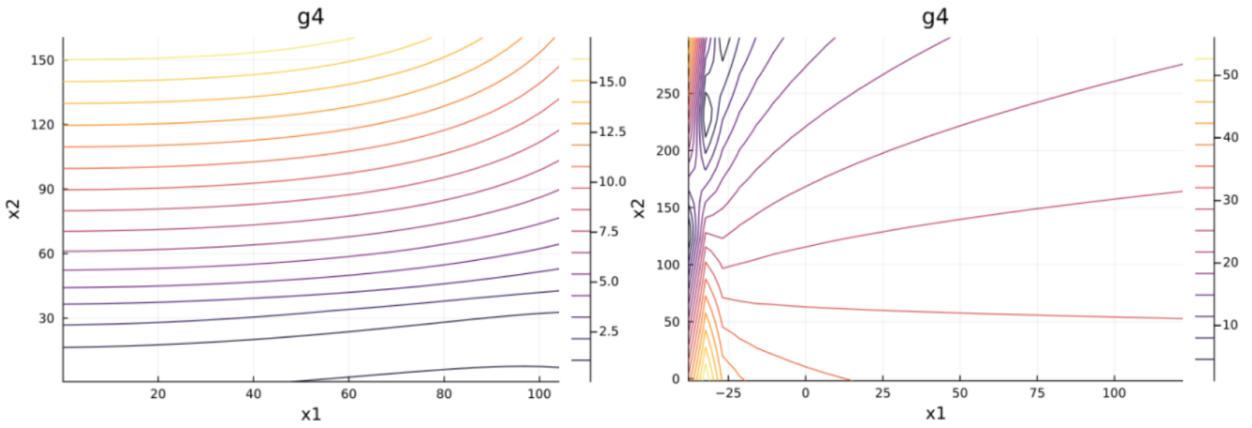

Fig. 9 Comparison of a section of the design space for nested optimization method (left) and shooting method (right). Contours show the value of the stall constraint.

1. Cessna-210

Using the methods described above, a trajectory optimization of the Cessna-210 aircraft model was performed. The trajectory was a velocity and altitude transition maneuver and it was optimized using one spline point for velocity and one spline point for altitude. Note again that the beginning and end points of the spline are fixed, and the spline point is placed in the middle of the trajectory. The results of this trajectory optimization are shown in Fig. 10.

This trajectory optimization converged in only 12 iterations. Considering most traditional methods require hundreds of function calls, this is about an order of magnitude speed up. In this trajectory, there is an initial portion of time with high accelerations, followed by more gradual changes in state and control input.

2. eVTOL Configuration

The eVTOL configuration was also simulated using the VPM to capture unsteady effects and wake interactions during a hover to cruise transition maneuver. Due to the fact that this maneuver was much longer and required more discretization than the previous example, only the inner loop optimal control was performed on this aircraft. Akima splines were defined to command forward velocity, and pitch of the aircraft, and control inputs where optimized to follow the commanded path. The results of this simulated maneuver are shown in Figs. 11 and 12

The resulting trajectory shows that lifting rotors maintain significant velocity for much of the trajectory, as the pusher rotor increases to accelerate the aircraft forward. As the system picks up speed, the wing provides more lift and the lifting rotors gradually drop off. The front rotors don't decrease as much as the rear rotors however, because they must provide enough moment to counteract the negative pitching moment from the tail.

V. Conclusion

This paper discussed and outlined a trajectory optimization using mid and high fidelity models. The optimization was able to successfully produce minimal energy trajectories by employing a novel nested optimization scheme. In this scheme, an outer loop optimized full vehicle states throughout the trajectory, and an inner loop calculated optimal control inputs to achieve those prescribed states. This method showed great improvements over the shooting method in terms of number of objective function evaluations, reliability of convergence, and optimality of the solution. In high computational cost scenarios, this method will ensure a relatively fast and robust solution.

Furthermore, the comparison between aerodynamic modeling techniques provided useful insights about the possibilities of modeling these aircraft, including the strengths and weaknesses of the VLM-BEMT and the VPM. It was shown that these two methods demonstrated reasonable agreement, but that the VPM captured forces that were caused by wake interactions that the VLM-BEMT did not resolve. These unsteady, oscillatory forces were most notable on the lifting rotors, and lifting surfaces of the Aurora PAV, especially as it increased forward velocity during a takeoff transition. The result suggests that unsteady effects and wake interaction may be important for maneuvers such as the Aurora PAV takeoff transition.

Future work in this area will include the following.

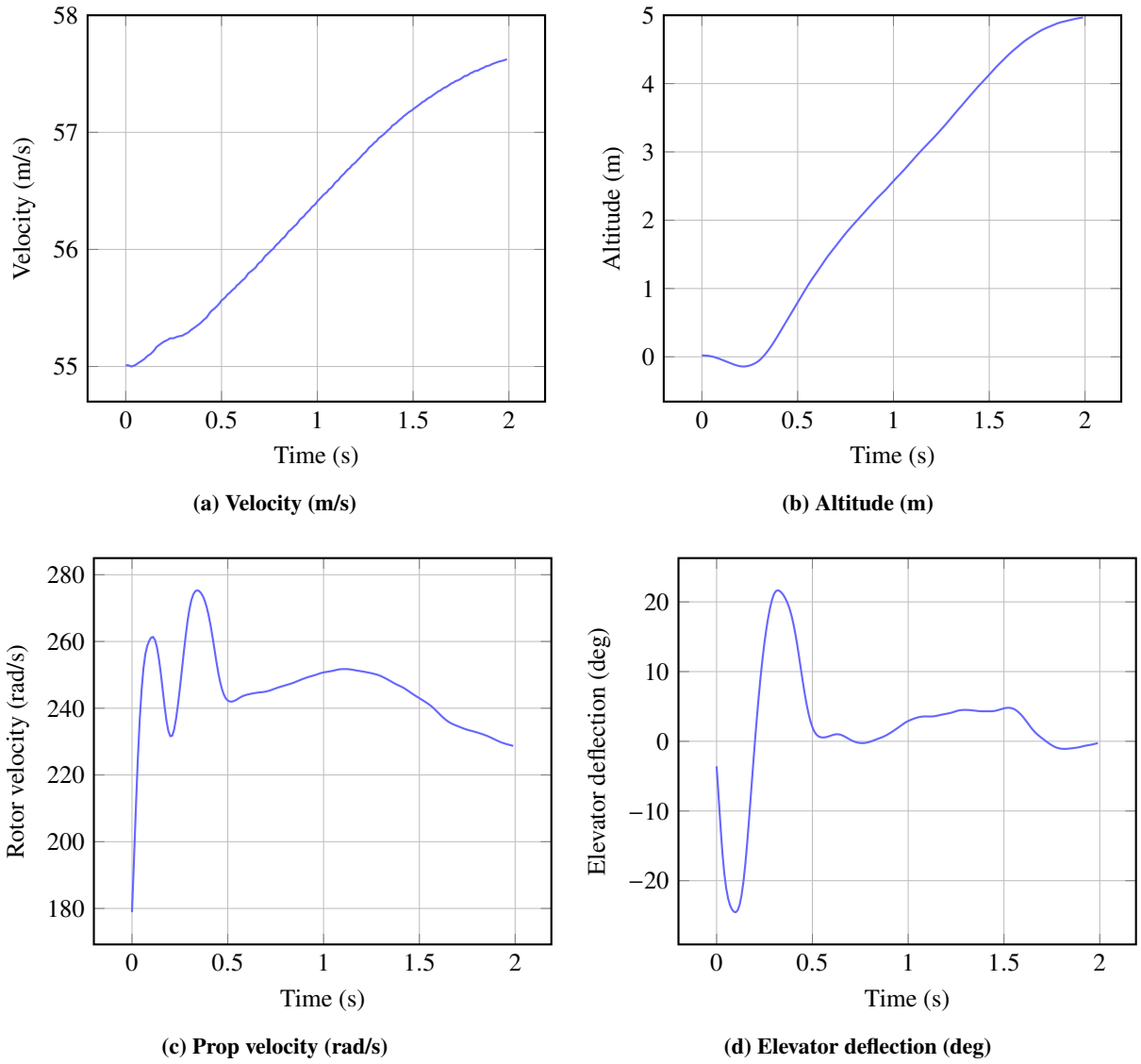

(a) Velocity (m/s)

(b) Altitude (m)

(c) Prop velocity (rad/s)

(d) Elevator deflection (deg)

Fig. 10 Trajectory Optimization of the Cessna-210 velocity and altitude transition

- Smoothing of optimal control inputs when used with the VPM
- Implementation of the full nested optimization for the Aurora PAV testcase
- Improvements to the robustness of the VPM in handling noisy gradients
- Improvements to the optimal control scheme

Resulting from this project was the development of a generalized trajectory optimization tool written in the Julia language. This tool is able to produce optimal control inputs for a given aircraft geometry and mission statement by applying a user selected aerodynamic model. This trajectory optimization platform is an example of the possibilities that can be realized when utilizing next-generation aerodynamic methods such as the VPM to design and control modern eVTOL aircraft.

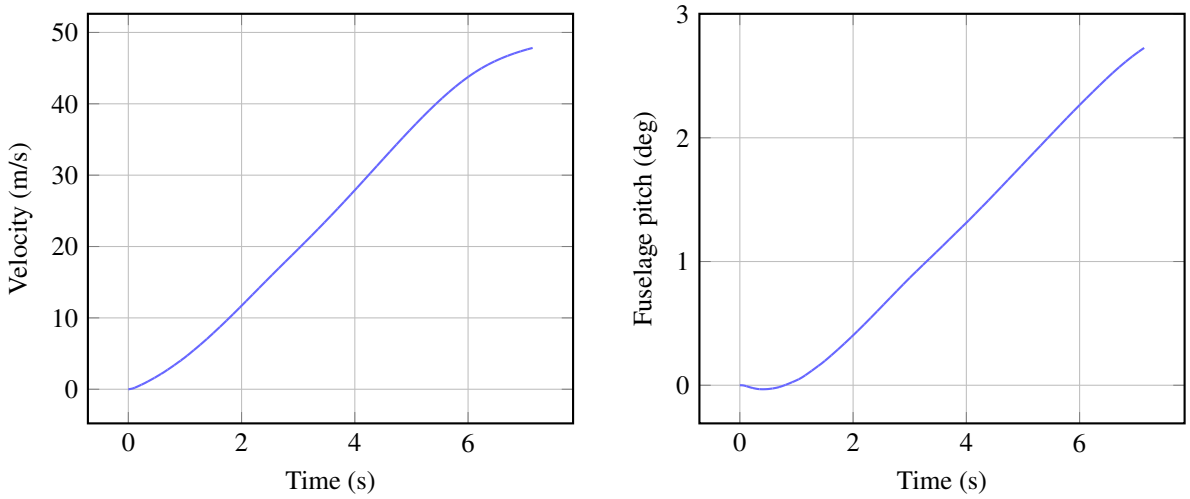

(a) Velocity (m/s) **(b) Fuselage pitch (deg)**

Fig. 11 Hover to cruise transition of the eVTOL using optimal control

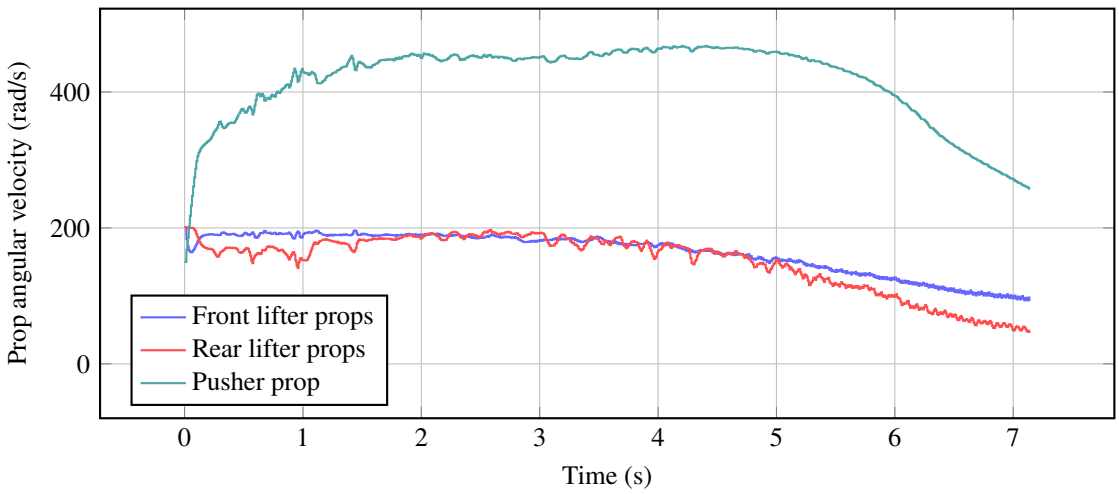

Fig. 12 Control inputs for hover to cruise transition of the eVTOL using optimal control

References

[1] Yeh, S.-T., and Du, X., "Optimal Tilt-Wing eVTOL Takeoff Trajectory Prediction Using Regression Generative Adversarial Networks," *Mathematics*, Vol. 12, No. 1, 2023, p. 26. https://doi.org/10.3390/math12010026, URL http://dx.doi.org/10.3390/math12010026.

[2] Flanzer, T., Bunge, R., and Kroo, I., "Efficient Six Degree of Freedom Aircraft Trajectory Optimization with Application to Dynamic Soaring," *12th AIAA Aviation Technology, Integration, and Operations (ATIO) Conference and 14th AIAA/ISSMO Multidisciplinary Analysis and Optimization Conference*, American Institute of Aeronautics and Astronautics, 2012, pp. 1–10. https://doi.org/10.2514/6.2012-5622, URL http://dx.doi.org/10.2514/6.2012-5622.

[3] Wang, M., Zhang, S., and Holzapfel, F., "Multi-resolution Trajectory Optimization of eVTOL Aircraft Using Capacity Collocation," *Advances in Guidance, Navigation and Control. ICGNC 2022. Lecture Notes in Electrical Engineering*, 2023, pp. 739–749.

[4] Chauhan, S. S., and Martins, J. R. R. A., "Tilt-Wing eVTOL Takeoff Trajectory Optimization," *Journal of Aircraft*, Vol. 57, No. 1, 2020, p. 93–112. https://doi.org/10.2514/1.c035476, URL http://dx.doi.org/10.2514/1.C035476.

[5] Wang, M., Diepolder, J., Zhang, S., Söpper, M., and Holzapfel, F., "Trajectory optimization-based maneuverability assessment of eVTOL aircraft," *Aerospace Science and Technology*, Vol. 117, 2021, p. 106903. https://doi.org/10.1016/j.ast.2021.106903, URL http://dx.doi.org/10.1016/j.ast.2021.106903.

[6] Marzougui, T., Neuhaus, K., Labracherie, L., and Scalabrin, G., "Optimal sizing of hybrid electric propulsion system for eVTOL," *IOP Conf. Ser. Mater. Sci. Eng.*, Vol. 1226, No. 1, 2022, p. 012070.

[7] An, J.-H., Kwon, D.-Y., Jeon, K.-S., Tyan, M., and Lee, J.-W., "Advanced Sizing Methodology for a Multi-Mode eVTOL UAV Powered by a Hydrogen Fuel Cell and Battery," *Aerospace*, Vol. 9, No. 2, 2022, p. 71. https://doi.org/10.3390/aerospace9020071, URL http://dx.doi.org/10.3390/aerospace9020071.

[8] Wang, M., Chu, N., Bhardwaj, P., Zhang, S., and Holzapfel, F., "Minimum-Time Trajectory Generation of eVTOL in Low-Speed Phase: Application in Control Law Design," *IEEE Transactions on Aerospace and Electronic Systems*, Vol. 59, No. 2, 2023, pp. 1260–1275. https://doi.org/10.1109/TAES.2022.3198033.

[9] Pradeep, P., Lauderdale, T. A., Chatterji, G. B., Sheth, K., Lai, C. F., Sridhar, B., Edholm, K.-M., and Erzberger, H., "Wind-Optimal Trajectories for Multirotor eVTOL Aircraft on UAM Missions," *AIAA AVIATION 2020 FORUM*, American Institute of Aeronautics and Astronautics, 2020, pp. 1–10. https://doi.org/10.2514/6.2020-3271, URL http://dx.doi.org/10.2514/6.2020-3271.

[10] Anderson, R., Willis, J., Johnson, J., Ning, A., and Beard, R. W., "A Comparison of Aerodynamics Models for Optimizing the Takeoff and Transition of a Bi-wing Tailsitter," *AIAA Scitech 2021 Forum*, American Institute of Aeronautics and Astronautics, 2021, pp. 1–17. https://doi.org/10.2514/6.2021-1008, URL http://dx.doi.org/10.2514/6.2021-1008.

[11] Li, B., Sun, J., Zhou, W., Wen, C.-Y., Low, K. H., and Chen, C.-K., "Transition optimization for a VTOL tail-sitter UAV," *IEEE/ASME Transactions on Mechatronics*, Vol. 25, No. 5, 2020, pp. 2534–2545.

[12] Droandi, G., Syal, M., and Bower, G., "Tiltwing Multi-Rotor Aerodynamic Modeling in Hover, Transition and Cruise Flight Conditions," *AHS International 74th Annual Forum & Technology Display*, 2018, pp. 1–10.

[13] Robertson, D. K., and Reich, G. W., "3-D vortex particle aerodynamic modelling and trajectory optimization of perching manoeuvres," *54th AIAA/ASME/ASCE/AHS/ASC Structures, Structural Dynamics, and Materials Conference*, 2013, p. 1703.

[14] Katz, J., and Plotkin, A., *Low-Speed Aerodynamics*, Cambridge University Press, 2001. https://doi.org/10/hk24.

[15] Moore, K. R., and Ning, A., "Distributed Electric Propulsion Effects on Existing Aircraft Through Multidisciplinary Optimization," *2018 AIAA/ASCE/AHS/ASC Structures, Structural Dynamics, and Materials Conference*, American Institute of Aeronautics and Astronautics, 2018, pp. 1–15. https://doi.org/10.2514/6.2018-1652, URL http://dx.doi.org/10.2514/6.2018-1652.

[16] Alvarez, E. J., Mehr, J., and Ning, A., "FLOWUnsteady: An Interactional Aerodynamics Solver for Multirotor Aircraft and Wind Energy," *AIAA AVIATION 2022 Forum*, American Institute of Aeronautics and Astronautics, 2022, pp. 1–36. https://doi.org/10.2514/6.2022-3218, URL http://dx.doi.org/10.2514/6.2022-3218.

[17] Revels, J., Lubin, M., and Papamarkou, T., "Forward-Mode Automatic Differentiation in Julia," *arXiv:1607.07892 [cs.MS]*, 2016. URL https://arxiv.org/abs/1607.07892.